Tech Science Press

Terminal Sliding Mode Controllers for Hydraulic Turbine Governing System with Bifurcated Penstocks under Input Saturation

Ji Liang[1], Zhihuan Chen[2,*], Xiaohui Yuan[1,3,*], Binqiao Zhang[3] and Yanbin Yuan[4]

[1]School of Hydropower and Information Engineering, Huazhong University of Science and Technology, Wuhan, 430074, China
[2]School of Information Science and Engineering, Wuhan University of Science and Technology, Wuhan, 430081, China
[3]Hubei Provincial Key Laboratory for Operation and Control of Cascaded Hydropower Station, China Three Gorges University, Yichang, 443002, China
[4]School of Resource and Environmental Engineering, Wuhan University of Technology, Wuhan, 430070, China
*Corresponding Authors: Zhihuan Chen. Email: chenzhihuan_hust@163.com; Xiaohui Yuan. Email: yxh71@163.com

Abstract: Terminal sliding mode controller method is introduced to enhance the regulation performance of the hydraulic turbine governing system (HTGS). For the purpose of describing the characteristics of controlled system and deducing the control rule, a nonlinear mathematic model of hydraulic turbine governing system with bifurcated penstocks (HTGSBF) under control input saturation is established, and the input/output state linearization feedback approach is used to obtain the relationship between turbine speed and controller output. To address the control input saturation problem, an adaptive assistant system is designed to compensate for controller truncation. Numerical simulations have been conducted under fixed point stabilization and periodic orbit tracking conditions to compare the dynamic performances of proposed terminal sliding mode controllers and conventional sliding mode controller. The results indicate that the proposed terminal sliding mode controllers not only have a faster response and accurate tracking results, but also own a stronger robustness to the system parameter variations. Moreover, the comparisons between the proposed terminal sliding mode controllers and current most often used proportional-integral-differential (PID) controller, as well its variant NPID controller, are discussed at the end of this paper, where the superiority of the terminal sliding mode controllers also have been verified.

Keywords: Hydraulic turbine governing system; bifurcated penstock; sliding mode controller; terminal sliding mode controller; saturation compensator

1 Introduction

Hydropower is one of the most widely used renewable sources for power generation, which converts kinetic and gravitational energy from water flow into electric power through turbines and generators, and then transfer the converted power into the grid. It is crucial for the hydropower plant to generate nearly constant frequency and constant voltage consistent with the grid, thus two main control aspects, i.e., voltage control (reactive power control) and frequency control (active power control) [1,2], are proposed in hydropower plant's governing system, In this paper, we focus on the problem of frequency control.

Any sudden change in power demand from the network grid would lead to a mismatch between the output of hydro-generator developed torque and electric demand, which causes the generator frequency to deviate from its nominal value. The wicket gate with the hydraulic turbine governing system (HTGS) is used to compensate such deviations by adjusting water flow into the turbine through a predefined control signal.

The HTGS system is in nature a nonlinear system, and a variety of modeling process of different subparts in this system have been reported in many literatures [3–13], which is an important and hot topic nowadays. Chen et al. [3] put forward a nonlinear model of HTGS system with a surge tank, Xu et al. [4] proposed a multi-hydro model of HTGS system under the excitation of stochastic and shock load. Chen et al. [5,6] proposed a linear-matrix based model of HTGS system with a detailed turbine equation. Yuan et al. [7] proposed a prototype model of HTGS system with a two-order generator model and external noises. Guo et al. [8] proposed a mathematical model of HTGS system with an upstream surge tank and sloping ceiling tailrace tunnel. Li et al. [9] proposed a nonlinear model of HTGS system in the process of sudden load increase transient. Wang et al. [10] proposed a fractional-order Francis HTGS system with time delay. Zhang et al. [11] established a fast-slow model of HTGS system with different time-scale coupling. Liang et al. [12] put forward a nonlinear model of HTGS system with a straight-tube surge tank. Xu et al. [13] combined the mathematical models of hydro-turbine governing system with the shaft system. However, for most previous research, the attentions are mainly focused on the hydraulic turbine and generator. For the penstocks, the nonlinear characteristics of the penstocks are rarely referred in a complete HTGS system, and this motivates the current research, where the bifurcated penstock effect and control input saturation is considered to build a more precise mathematical model of HTGS system. Moreover, the second order generator sub-model and system uncertainties in [7] are also taken into account in the new model.

Accompanied with the modeling of the HTGS system, the control of HTGS system also suffers from many significant improvements. In the past, the parallel PID controller and its variants are the commonly used governor in HTGS, which have excellent performances in a small range around the linearized working points through some intelligence algorithms, but it always has poor ability to handle the system uncertain noises according to the results in [7,12,14]. Therefore, the hydro plant's performance usually decreases after prolong use. As the demand for energy is increasing nowadays, the HTGS system is in great need of modern advanced control methods that should not only perform well in maintaining the nominal frequency response but also be robust to the external disturbances and inner uncertainties at the abnormal working status.

Recently, many researchers have studied new control design methods for different mathematical models of the HTGS by applying modern control techniques, such as fuzzy logic control [15], predictive control [16,17] and neural network control [18]. There are also several studies based on sliding mode controller (SMC) techniques, see [7,14,19]. However, most current SMC methods for the hydropower system is on the basis of a linear structure, where the sliding mode surface is a linear combination of states constructed using appropriate time-invariant coefficients. The use of such coefficient makes sliding surface static evenly in the presence of system uncertainties, which contributes a lot to the strong robustness in controllers, but it easily leads to a sharp transient response around the equilibrium point of generator frequency change. Although the dynamic response can be improved by utilizing a balanced value for the linear surface functions through some effective tools such as saturation approximation function [7], and fuzzy logic strategy [14], the system states can only converge to the equilibrium point asymptotically. To further improve the system response, a direct way is to introduce some nonlinear sliding mode surfaces. One typical example of such nonlinear sliding mode surface based controllers is terminal sliding mode controller (TSMC), which can ensure the finite-time convergence of the response and has been demonstrated to possess some nice features such as a faster response, better robustness and disturbance rejection properties [20–22].

In this paper, two versions of TSMC, i.e. traditional terminal sliding mode controller (TTSMC) [23], and non-singular terminal sliding mode controller (NTSMC) [24], have been adopted for controlling the nonlinear hydraulic turbine governing system with bifurcated penstocks (HTGSBF), a special mathematical model of the HTGS system that considers the effects of bifurcated penstocks and system uncertainties under control input saturation. The ideas behind these two methods are to form an exponential sliding surface that assures a finite time convergence to the equilibrium point. Besides that, in order to overcome the inherent control input saturation caused by the guide vane opening limit, a novel control compensator has been incorporated into TTSMC and NTSMC controller. This compensator is a two-order system in essential, which has been proved to track the truncation error accurately through Lyapunov stability analysis. System responses and controller efforts have been evaluated. The results indicate that these two types TSMC controllers outperform conventional SMC controller in terms of the regulation quality and tracking errors in all simulation cases. Moreover, comparing to the PID and NPID controllers, the proposed TTSMC and NTSMC controllers also show tremendous advantages in terms of maximum tracking errors, average tracking errors, and standard deviations of tracking errors in all simulation cases.

Accordingly, the main contributions of this paper can be summarized as follows:

1. A new mathematical model of HTGS system that considers the effects of the bifurcated penstock and system uncertainties (HTGSBF) under control limitation is proposed in this study.
2. The terminal sliding mode control schemes are first introduced into the governor design of HTGS system to offer faster response speed and better regulation accuracy.
3. A novel two-order control compensator is put forward in the existence of nonlinear saturation component in HTGSBF model to balance the truncation error caused by the designed output and actual output.
4. The strict finite-time convergence and stability analysis for the HTGSBF model with two designed terminal sliding mode controllers have been verified by finite-time theory and Lyapunov stability theory.

The rest of this paper is organized as follows. The modeling of the HTGS system with bifurcated penstocks is described in Section 2. The methods of three sliding mode controllers for the HTGSBF model based on input/output state feedback linearization method and saturation compensator are illustrated in Section 3. The comparative experiments are presented in Section 4. The discussions and conclusions are summarized in Section 5 and Section 6, respectively.

2 Mathematical Model of HTGS System

Owing to the different natural conditions of various hydropower plants, there is not a universal and effective model available for all HTGS systems around the world. A lot of pioneering works with respect to the models of the HTGS have been made in recent years. Among them, we can roughly divided the existing models into two classes: the first one is linear models [5,6,25,26], which usually constructs the relationships of different hydro devices through a linear control matrix. In these works, the transfer functions of the generator are always described by a one-order differential equation, and the nonlinear characters of the penstock and the turbine are ignored; the second one is nonlinear models, which pay attentions on the nonlinearities of the hydro plants, especially for high-order generator sub-models [3,4,7–12,27].

Generally, the hydropower plant consists of a reservoir, dam, penstocks, turbine, generator, draft tube, and power house connected to the grid as shown in Fig. 1. One of the most important components of a typical hydro plant is the penstocks [28]. In general, there are two types of penstocks, i.e., single penstock and bifurcated (or sharing) penstocks. The single penstock is just connected with an independent hydro-generator unit, and bifurcated penstocks are usually connected with multi-hydro-generator units. In this
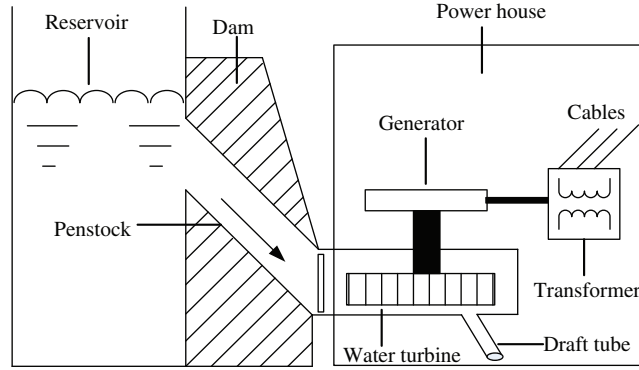
Figure 1: Typical hydropower station scheme

research, we focus on the bifurcated/sharing penstocks, and establish a new mathematical model of the HTGS system as follows.

2.1 Hydraulic Turbine

In the neighborhood of a specific operating point, the equation of the turbine is expressed as [5]:

$$\begin{pmatrix} m_t \\ q \end{pmatrix} = \begin{pmatrix} e_x \\ e_{qx} \end{pmatrix} x_t + \begin{pmatrix} e_y \\ e_{qy} \end{pmatrix} y + \begin{pmatrix} e_h \\ e_{qh} \end{pmatrix} h \tag{1}$$

where m_t, q, x_t, y, and h are the turbine torque, turbine flow, turbine speed deviation, guide vane opening deviation, and water head deviation, respectively. The coefficients e_x, e_y, e_h, e_{qx}, e_{qy} and e_{qh} are the partial derivatives of turbine torque and turbine flow with respect to the turbine speed deviation, guide vane opening deviation, and water head deviation, i.e., $e_x = \dfrac{\partial m_t}{\partial x_t}$, $e_y = \dfrac{\partial m_t}{\partial y}$, $e_h = \dfrac{\partial m_t}{\partial h}$, $e_{qx} = \dfrac{\partial q}{\partial x_t}$, $e_{qy} = \dfrac{\partial q}{\partial y}$, $e_{qh} = \dfrac{\partial q}{\partial h}$. These coefficients vary as the operating point changes. According to the turbine synthetic characteristic curve, six detailed expressions about these derivatives can be given as follows [3,10]:

$$e_x = e_{xm}\sqrt{(h+1)}, \ e_y = e_{ym}(h+1), \ e_h = e_{hm}, e_{qx} = e_{qxm}, \ e_{qy} = e_{qym}\sqrt{(h+1)}, \ e_{qh} = e_{qhm}/(x_t+1) \tag{2}$$

where e_{xm}, e_{ym}, e_{hm}, e_{qxm}, e_{qym} and e_{qhm} are the basis partial derivatives of hydraulic turbine around a small disturbance at the rated working conditions, and then (1) can be deduced as:

$$\begin{cases} m_t = e_{xm}\sqrt{(h+1)}x_t + e_{ym}(h+1)y + e_{hm}h \\ q = e_{qxm}x_t + e_{qym}\sqrt{(h+1)}y + e_{qhm}h/(x_t+1) \end{cases} \tag{3}$$

2.2 Bifurcated Penstocks

The bifurcated penstocks, as shown in Fig. 2, are used to lead the water into different pipeline branches through the water conveyance tunnel and common penstock before arriving at the bifurcation point.

As the length of common penstocks usually short, and the flow in common penstock changes slowly, the models of the penstock system can be considered as a rigid water hammer plant, and the working conditions of hydro-generator units depend on the flow in *ith* bifurcated penstock, which can be represented as [4]:
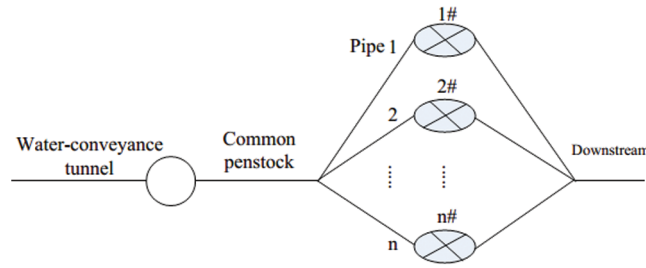
Figure 2: The sketch of the bifurcated penstock

$$\frac{h(s)}{q(s)} = -\frac{(T_{wp} + T_{wi})s}{1 + \dfrac{T_{wp}T_{wi}s^2}{4h_{wi}^2}} \tag{4}$$

where T_{wp} is the time constant of common penstock, T_{wi} and h_{wi} are the time constant and intrinsic coefficient of ith penstock, respectively.

Substituting (3) into (4), then the results can be written in state-space form as:

$$\begin{cases} \dot{x}_1 = x_2 - b_1 q = x_2 - b_1[e_{qxm}\,x_t + e_{qym}\sqrt{(h+1)}y + e_{qhm}h/(x_t+1)] \\ \dot{x}_2 = -a_1 x_1 \end{cases} \tag{5}$$

where x_1 and x_2 are the intermediate variables, $a_1 = \dfrac{4h_{wi}^2}{T_{wp}T_{wi}}$, $b_1 = \dfrac{4h_{wi}^2(T_{wp} + T_{wi})}{T_{wp}T_{wi}}$, and $h = x_1$.

2.3 Hydraulic Servo System

The servo system, as the actuator of hydraulic turbine, is used to amplify the control signal [8]. In most literatures, it always simplified as a one-order inertial system. However, for the actual situation, the output of the controller u is strictly limited to a certain range [6], which mainly due to the finite opening range of wicket gate system. The mathematical expression of this system is as follows:

$$\dot{y} = \frac{1}{T_y}(u - y), \quad u = sat(v) \tag{6}$$

where T_y is the servo system time constant, u is the actual control input to the system that is constrained in a certain range. Assuming that v is the control output to be designed in this study. The relationship of v and u can be expressed as: $u = sat(v) = \begin{cases} sign(v)u_{max}, & if \ |v| > u_{max} \\ v, & if \ |v| \leq u_{max} \end{cases}$ with u_{max} being a positive constant that quantizes the bound of control input saturation.

2.4 Generator System

A second-order mathematical model of synchronous generator unit is used to study the dynamic behavior of the hydro plant generator system [9]. The differential equations of it are as follows:

$$\begin{cases} \dot{\delta} = \omega_0 x_t \\ \dot{x}_t = \dfrac{1}{T_a}(m_t - m_e - Dx_t) \end{cases} \tag{7}$$

where δ, T_a, m_e, D and ω_0 denote the rotor angle, mechanical starting time constant, electro-magnetic torque, damping coefficient of the generator, and the base angular speed of the grid, respectively. Ignoring the tiny friction loss, the mechanical torque of the synchronous generator m_e is equal to its electromagnetic power P_e,

$$m_e = P_e = \frac{E_q' V_s}{\tau_d} \sin \delta + \frac{V_s^2}{2} \frac{\tau_d - \tau_q}{\tau_d \tau_q} \sin(2\delta) \tag{8}$$

where τ_d and τ_q are the reactance of direct axis and quadrature axis, E_q' is the generator transient voltage of quadrature axis, and V_s is the generator voltage of infinite bus system.

Considering the uncertain interactions among the hydraulic, mechanical, and electrical devices, the equations of hydraulic turbine governing system with bifurcated penstocks (HTGSBF) are given as:

$$\begin{cases} \dot{x}_1 = x_2 - b_1 \left(e_{qxm} x_5 + e_{qhm} \dfrac{x_1}{x_5 + 1} + e_{qym} x_3 \sqrt{x_1 + 1} \right) + d_1 \\ \dot{x}_2 = -a_1 x_1 + d_2 \\ \dot{x}_3 = \dfrac{1}{T_y} (u - x_3) + d_3, \quad u = sat(v) \\ \dot{x}_4 = w_0 x_5 + d_4 \\ \dot{x}_5 = \dfrac{1}{T_a} \left\{ e_{xm} x_5 \sqrt{x_1 + 1} + e_{hm} x_1 + e_{ym} x_3 (x_1 + 1) - \dfrac{E_q' V_s}{\tau_d} \sin(x_4) - \dfrac{V_s^2}{2} \dfrac{\tau_d - \tau_q}{\tau_d \tau_q} \sin(2x_4) - D x_5 \right\} + d_5 \end{cases} \tag{9}$$

where $x_3 = y$, $x_4 = \delta$ and $x_5 = x_t$, d_1-d_5 denote bounded system uncertainties (including the modeling errors caused by assumptions, un-modeled nonlinearities, inner perturbations, and external noises, etc.). $Y = x_5$ is the hydraulic turbine rotational speed, which is also commonly referred to the generator frequency change or the system output. It notes that the bifurcated penstock in HTRSBF are connected to other turbines, which results to different values of a_1 and b_1 for different sub-penstocks. In this study, for the sake of simplicity, we just selected the 1-th bifurcated penstock as an example.

3 Controller Design for the HTGSBF Model

In this section, the synthesis of three different sliding mode controller design methods for the HTGSBF model based on input/output state linearization feedback method and control input saturation compensator are presented as follows.

3.1 Input/Output State Linearization Feedback of the HTGSBF

The main control task of the HTGSBF is to lead the output of $Y(t)$ (i.e., x_5) approaching to the desired output $Y_d(t)$ (i.e., x_d). In (9), it is seen that there is not any direct relationship between Y and u, thus the input/output state linearization feedback method [7] is adopted to construct the linear model of the HTGSBF. Differentiating Y (i.e., x_5) with respect to time, we obtain the following formula.

$$\dot{Y} = \dot{x}_5 = \frac{1}{T_a} \left\{ e_{xm} x_5 \sqrt{x_1 + 1} + e_{hm} x_1 + e_{ym} x_3 (x_1 + 1) - \frac{E_q' V_s}{\tau_d} \sin(x_4) \right.$$
$$\left. - \frac{V_s^2}{2} \frac{\tau_d - \tau_q}{\tau_d \tau_q} \sin(2x_4) - D x_5 \right\} + d_5 \tag{10}$$

$$\ddot{Y} = \ddot{x}_5 = \frac{1}{T_a}\{(\frac{e_{xm}x_5}{2\sqrt{x_1+1}} + e_{ym}x_3 + e_{hm})f_1 - e_{ym}(x_1+1)f_3 - [\frac{E_q'V_s}{\tau_d}\cos(x_4) + \frac{V_s^2(\tau_d-\tau_q)}{\tau_d\tau_q}\cos(2x_4)]f_4$$

$$- (D - e_{xm}\sqrt{x_1+1})f_5\} + \frac{e_{ym}(x_1+1)}{T_aT_y}u + \frac{1}{T_a}\{(\frac{e_{xm}x_5}{2\sqrt{x_1+1}} + e_{ym}x_3 + e_{hm})d_1 + e_{ym}(x_1+1)d_3 \quad (11)$$

$$- [\frac{E_q'V_s}{\tau_d}\cos(x_4) + (\frac{1}{\tau_q}-\frac{1}{\tau_d})V_s^2\cos(2x_4)]d_4 - (D - e_{xm}\sqrt{x_1+1})d_5\} + \dot{d}_5 = f + b*u + d_m$$

where the nonlinear function item $f_1 = x_2 - b_1(e_{qxm}x_5 + e_{qhm}\dfrac{x_1}{x_5+1} + e_{qym}x_3\sqrt{x_1+1}), f_3 = \dfrac{x_3}{T_y}, f_4 = w_0x_5,$

$$f_5 = \frac{1}{T_a}\{e_{xm}x_5\sqrt{x_1+1} + e_{hm}x_1 + e_{ym}x_3(x_1+1) - \frac{E_q'V_s}{\tau_d}\sin(x_4) - \frac{V_s^2}{2}\frac{\tau_d-\tau_q}{\tau_d\tau_q}\sin(2x_4) - Dx_5\}, \text{ and}$$

$$f = \frac{1}{T_a}\{e_{ym}(x_1+1)f_3 + (e_{ym}x_3 + \frac{e_{xm}x_5}{2\sqrt{x_1+1}} + e_{hm})f_1 - [\frac{E_q'V_s}{\tau_d}\cos(x_4) + \frac{V_s^2(\tau_d-\tau_q)}{\tau_d\tau_q}\cos(2x_4)]f_4 - (D-$$

$e_{xm}\sqrt{x_1+1})f_5\}$. The control coefficient $b = \dfrac{e_{ym}(x_1+1)}{T_aT_y}$; The item $d_m = \dfrac{1}{T_a}\left\{(\dfrac{e_{xm}x_5}{2\sqrt{x_1+1}} + e_{hm} + e_{ym}x_3)\right.$

$$d_1 + e_{ym}(x_1+1)d_3 - [\frac{E_q'V_s}{\tau_d}\cos(x_4) + \frac{V_s^2(\tau_d-\tau_q)}{\tau_d\tau_q}\cos(2x_4)]d_4 - (D - e_{xm}\sqrt{x_1+1})d_5\} + \dot{d}_5$$

3.2 Control Input Saturation Compensator

Due to the control output limitation, u is usually bounded as shown in Fig. 3. It is obvious that there is a truncation error between the control input demand v and actual output u because of the saturation component. In order to address this issue, a saturation compensator is designed and adopted in HTGSBF model as shown in Fig. 3.
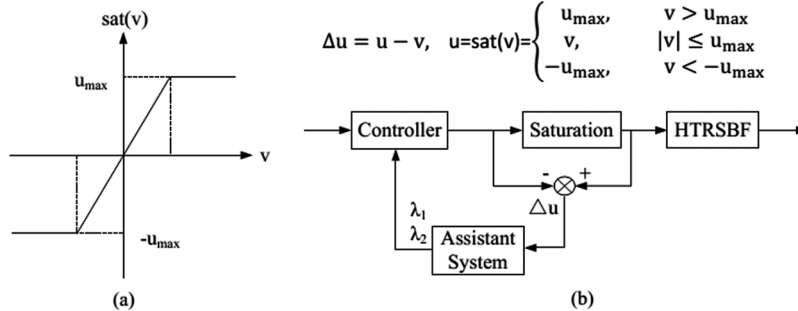

$$\Delta u = u - v, \quad u = sat(v) = \begin{cases} u_{max}, & v > u_{max} \\ v, & |v| \le u_{max} \\ -u_{max}, & v < -u_{max} \end{cases}$$

(a) (b)

Figure 3: The scheme diagram of control input saturation compensator

The main idea of saturation compensator is based on an adaptive assistant system, which is described as:

$$\begin{cases} \dot{\lambda}_1 = -c_1\lambda_1 + \lambda_2 \\ \dot{\lambda}_2 = -c_2\lambda_2 + b\Delta u \end{cases} \quad (12)$$

where λ_1 and λ_2 are two state vectors. In essence, the compensator is a specified amplifier that enlarges the value of control output error Δu ($\Delta u = u - v$). To facilitate the controller stability design of the assistant system, (12) can be formally written as:

$$\dot{\boldsymbol{\lambda}} = \mathbf{A}\boldsymbol{\lambda} + \mathbf{B}\Delta u \quad (13)$$

where $\boldsymbol{\lambda} = \begin{pmatrix} \lambda_1 \\ \lambda_2 \end{pmatrix}$, $\mathbf{A} = \begin{pmatrix} -c_1 & 1 \\ 0 & -c_2 \end{pmatrix}$, and $\mathbf{B} = \begin{pmatrix} 0 \\ b \end{pmatrix}$. To ensure $\lim_{t \to \infty} \lambda_i(t) \to 0$, the matrix $\mathbf{A}$ needs to be a Hurwitz matrix, thus $c_1 > 0$, $c_2 > 0$. In order to combine the designed saturation compensator into the controller, some extra criteria that ensure the Lyapunov stability of the system should be analyzed, which will be introduced in the following part.

3.3 Sliding Mode Controller Design

In this part, we will present three different controller designs based on the above saturation compensator (12), which includes the conventional sliding mode controller (CSMC), traditional terminal sliding mode controller (TTSMC) and non-singular terminal sliding mode controller (NTSMC). As enunciated in [29], the design of sliding mode controllers can be divided into two parts: a continuous control signal (usually called equivalent control) which controls the system when its states are on the sliding manifold, and a discontinuous control signal which handles the system uncertainties and external disturbance (usually called switching control). More details about each controller for the HTGSBF model are provided as follows.

1) Conventional sliding mode controller (CSMC)

For the conventional sliding mode controller, a linear sliding surface function can be expressed as:

$$e = x_5 - x_d - \lambda_1, \quad s = ce + \dot{e} \tag{14}$$

and a commonly used switching item, i.e. the switching control signal, can be designed as [7]:

$$u_{sw} = -\frac{k_1}{b}\text{sgn}(s) \tag{15}$$

where c and k_1 are two positive constants. The value of k_1 is greater than the upper bound of system uncertainties, i.e., $k_1 > D_r$, $D_r = \max_{t:\, 0 \to \infty} |d_m(t)|$. By differentiating the sliding surface s with respect to time, we obtain:

$$\dot{s} = c\dot{e} + \ddot{e} = c\dot{e} - \ddot{x}_d + f + bv + d_m - c_1^2\lambda_1 + (c_1 + c_2)\lambda_2 \tag{16}$$

According to the equivalent control design of sliding mode control [29], we can design the total controller output v for the HTGSBF model as follows:

$$v = -\frac{1}{b}(c\dot{e} - \ddot{x}_d + f + \Phi + k_1\text{sgn}(s)) \tag{17}$$

where the function $\Phi = -c_1^2\lambda_1 + (c_1 + c_2)\lambda_2$, and $\text{sgn}(s)$ is defined as follows: $\text{sgn}(s) = 1$, if $s > 0$; $\text{sgn}(s) = 0$, if $s = 0$; $\text{sgn}(s) = -1$, if $s < 0$.

Theorem 1: Under the control output v defined in (17), the sliding surface (14) is attractive and invariant.

Proof 1: We select the following Lyapunov function:

$$V = \frac{1}{2}s^2 \tag{18}$$

On the basis of (16) and (17), we get:

$$\dot{V} = s\dot{s} = s(d_m - k_1\text{sgn}(s)) \leq (d_m - k_1)|s| \leq 0 \tag{19}$$

which implies the attractiveness of the surface (14). Moreover, since $\lim_{s \to 0} s\dot{s} = 0$, the surface (14) is invariant.

In order to guarantee the condition $x_5 \to x_d$, $\lambda_i \to 0$ is needed. Thus, the validity of the compensator depends on whether the criterion $\lambda_i \to 0$ is satisfied. According to (12), if Δu is bounded, the criterion $\lambda_i \to 0$ will be satisfied. Then the validity of the designed saturation compensator is transferred into verifying the criterion

whether Δu is bounded. In this study, we assure that v is bounded, hence Δu is bounded. Therefore, (13) is stable, and $\lim_{t \to \infty} \lambda_i(t) \to 0$ will be guaranteed through finding a proper value of c_i.

2) Traditional terminal sliding mode controller

Similar to CSMC, the traditional terminal sliding controller needs to define a special variable surface called traditional terminal sliding surface in the form [23]:

$$s = \dot{e} + \beta e^{\frac{q_1}{p_1}} \tag{20}$$

where $\beta > 0$, p_1 and q_1 are two positive odd integers such that $p_1 > q_1$. The traditional terminal sliding mode controller for the HTGSBF model can be designed as:

$$v = -\frac{1}{b}(f - \ddot{x}_d + \Phi + k_2 \text{sgn}(s) + \beta \frac{q_1}{p_1} e^{\frac{q_1}{p_1} - 1} \dot{e}) \tag{21}$$

where $k_2 > D_r$, and $\delta = k_2 - D_r$ is a positive constant.

Theorem 2: The sliding mode surface (20) is attractive and invariant with the control output defined in (21).

Proof 2: Differentiating the sliding mode surface s with respect to time, we can get:

$$\dot{s} = \ddot{e} + \beta \frac{q_1}{p_1} e^{\frac{q_1}{p_1} - 1} \dot{e} \tag{22}$$

According to (11) and (14), (22) can be deduced as,

$$\dot{s} = f + bu + d_m - \ddot{x}_d - \dot{\lambda}_1 + \beta \frac{q_1}{p_1} e^{\frac{q_1}{p_1} - 1} \dot{e} \tag{23}$$

Substituting (13) and (21) into (23), we can get and the following expression:

$$s\dot{s} = (d_m - k_2 \text{sgn}(s))s \leq (D_r - k_2)|s| = -\delta|s| \leq 0 \tag{24}$$

Hence, the sliding surface (20) is attractive and invariant with the control output defined in (21).

Theorem 3: The generator frequency change error of the HTGSBF converges to zero in finite time.

Proof 3: Supposing that t_r is the time from $s(0) \neq 0$ to $s = 0$, i.e., $s(t_r) = 0$, which satisfies [20]:

$$\dot{s} = -\delta \frac{|s|}{s} = \pm \delta \tag{25}$$

Then it follows:

$$\int_{s=s(0)}^{s=s(t_r)} ds = \int_{t=0}^{t=t_r} \pm \delta dt \tag{26}$$

and t_r can be deduced as:

$$t_r = \left| \frac{s(0)}{\delta} \right| = \frac{|s(0)|}{\delta} \tag{27}$$

where the terminal sliding mode state $s(t_r) = 0$ is reached, the system dynamic behavior of $\dot{e}$ can be determined by the following nonlinear dynamic equation:

$$\dot{e} + \beta e^{\frac{q_1}{p_1}} = 0 \tag{28}$$

Based on (28), a finite time interval t_s, which is taken from $e(t_r) \neq 0$ to $e(t_r + t_s) = 0$, can be obtained as follows:

$$t_s = \frac{p_1}{\beta(p_1 - q_1)} |e(t_r)|^{(1-\frac{q_1}{p_1})} \tag{29}$$

which denotes that both the tracking error e and its derivative $\dot{e}$ of the HTGSBF model (i.e., the controlled system) will converge to zero in a finite time $(t_s + t_r)$.

3) Nonsingular terminal sliding mode controller

To avoid the singularity issue when $e = 0$ and $\dot{e} \neq 0$ in terminal sliding mode controller, a nonsingular terminal sliding mode surface is defined as [24]:

$$s = e + \frac{1}{\alpha} \dot{e}^{\frac{p_2}{q_2}} \tag{30}$$

where $\alpha > 0$, p_2 and q_2 are two positive odd integers, and $1 < \frac{p_2}{q_2} < 2$. The nonsingular terminal sliding mode controller for the HTGSBF model can be designed as:

$$v = -\frac{1}{b}(f - \ddot{x}_d + \Phi + k_3 \mathrm{sgn}(s) + \alpha \frac{q_2}{p_2} \dot{e}^{2-\frac{p_2}{q_2}}) \tag{31}$$

where $k_3 > D_r$, and $\eta = k_3 - D_r$ is a positive constant.

Theorem 4: The sliding mode surface (30) can ensure a finite time convergence to the equilibrium point of the HTGSBF model.

Proof 4: Choosing the following Lyapunov function $V = \frac{1}{2}s^2$, its time derivative is:

$$\dot{V} = s(\dot{e} + \frac{1}{\alpha}\frac{p_2}{q_2}\dot{e}^{\frac{p_2}{q_2}-1}\ddot{e}) = s[\dot{e} + \frac{1}{\alpha}\frac{p_2}{q_2}\dot{e}^{\frac{p_2}{q_2}-1}(f + bu + d_m - \ddot{x}_d - \dot{\lambda}_1)] = \frac{1}{\alpha}\frac{p_2}{q_2}\dot{e}^{\frac{p_2}{q_2}-1}(d_m s - k_3|s|) \tag{32}$$

Since that p_2 and q_2 are two positive odd integers, we have $\dot{e}^{\frac{p_2}{q_2}-1} \geq 0$, and considering that $d_m < k_3$, we obtain:

$$s\dot{s} \leq \frac{1}{\alpha}\frac{p_2}{q_2}\dot{e}^{\frac{p_2}{q_2}-1}(d_m|s| - k_3|s|) = -\frac{1}{\alpha}\frac{p_2}{q_2}\dot{e}^{\frac{p_2}{q_2}-1}\eta|s| \leq 0 \tag{33}$$

and two different situations are discussed as follows:

i)   when $\dot{e} \neq 0$, it satisfies $\dot{V} = s\dot{s} < 0$, hence the system (11) with the controller (31) is stable.

ii) when $\dot{e} = 0$, from (30), we get $e \neq 0$ when $s \neq 0$, which means that the deviations of state variables are not always at the equilibrium point, and continue to across the axis $\dot{e} = 0$ in the $(e, \ \dot{e})$ plane, but s is not always equal to zero. Since that $\ddot{e} = \alpha\frac{q_2}{p_2}\dot{e}^{2-\frac{p_2}{q_2}} + d_m - k_3\mathrm{sgn}(s)$, we have $\ddot{e} < -\eta$ when $s > 0$, i.e., $\dot{e}$ decreases quickly; and when $s < 0$, we have $\ddot{e} > \eta$, i.e. $\dot{e}$ increases quickly. The phase portrait of HTGSBF model is then described as shown in Fig. 4. We can see that when $\dot{e} = 0$, the HTGSBF model (9) with the designed controller (31) will reach the manifold $s = 0$ in a finite time.
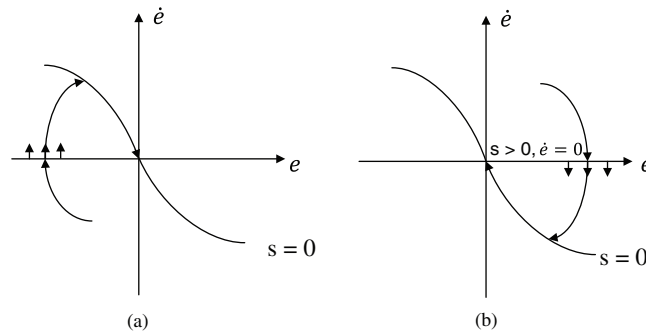
Figure 4: The phase plot of NTSMC controller when $\dot{e} = 0$. (a) $s < 0$, $\dot{e} = 0$. (b) $s > 0$, $\dot{e} = 0$

3.4 Implementation of Three Sliding Mode Controllers into HTGSBF

For the regulation of HTGSBF model, there are three difficulties in control design. Firstly, it should establish a direct correlation between controller output u and turbine rotational speed output x_t. Secondly, the output of the designed controller is bounded in a certain range due to the control limitation. Thirdly, there needs an anti-interface controller against the uncertainties d_m; To address these issues, three corresponding measurements, named the input/output state linearization feedback method listed in Section 3.1, control input saturation compensator listed in Section 3.2, and three sliding mode control design listed in Section 3.3 are introduced in this study. The implementation of our designed scheme is presented as shown in Fig. 5.
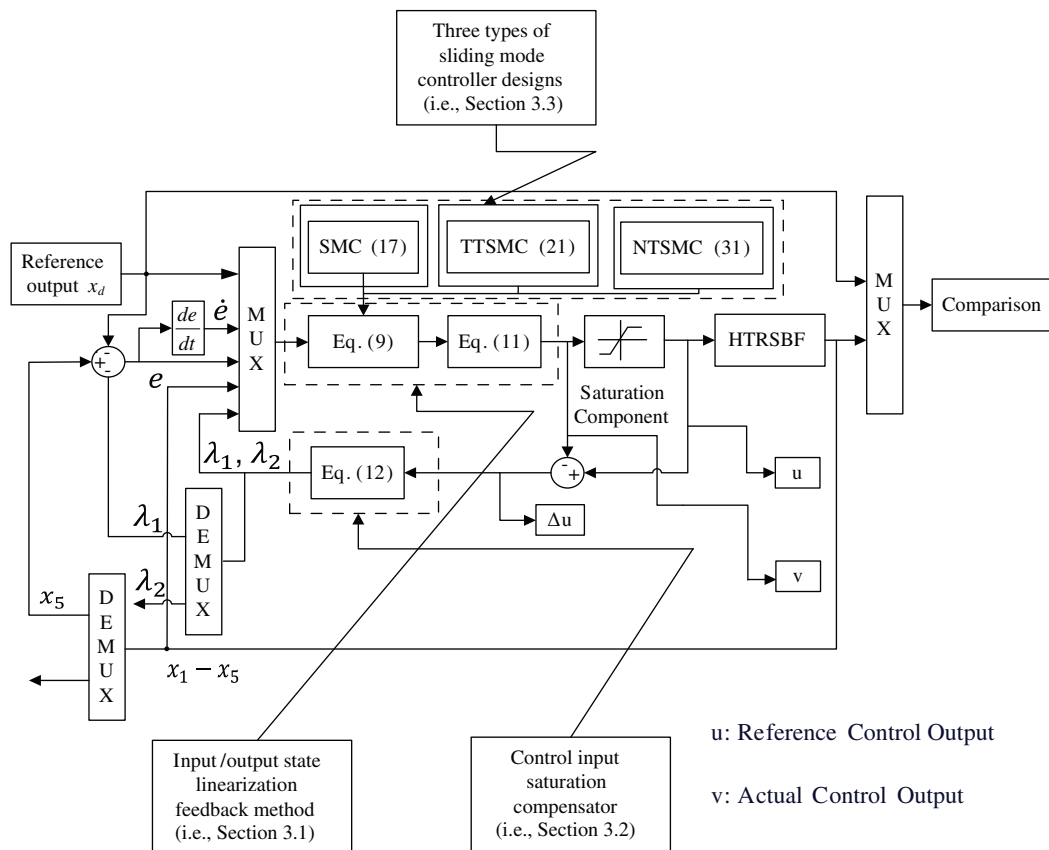

Figure 5: The block diagram of HTGSBF model with different sliding mode controllers

It is interesting to note that the terminal sliding mode controller uses so-called the finite-time convergence concept, and has been proven to have special merits on high stability and robustness to the un-modeled system uncertainties [30–32]. It is well-known that a linear sliding function generates exponential stability, and the state infinitely approaches, but can never reach the equilibrium. On the contrary, the terminal function enables a faster response and finite time convergence property because of the non-integer exponent. However, one major drawback of terminal sliding mode controller is the singularity issue due to the reason that the terms with negative fractional powers may exist. To overcome this problem, a new type of terminal sliding mode control techniques called nonsingular terminal sliding mode controllers is always used as shown in (30). The validity and effectiveness of the TTSMC and NTSMC, as well the CSMC controller will be verified in the following section.

4 Numerical Simulation Results

To demonstrate the performance of the proposed control schemes, simulations are conducted in MATLAB R2016a with a desktop computer of Intel Core i7-6600, 2.60 GHz CPU, 64-bit Windows 10 operating system. Three comparative sliding mode methods, i.e., CSMC, TTSMC and NTSMC controller, are applied to govern the output of HTGSBF model (9), respectively. The constants and the uncertainties of (9) are presented in Tab. 1 [33]. Note that all the uncertainties are sine and cosine functions with small amplitude, which is mainly due to the reason that the disturbance signals in hydro plant are usually generated by electro-magnetic devices. To have a fair comparison, the gains of CSMC, TTSMC, and NTSMC controllers are assigned as a same value, and the controller parameters are listed in Tab. 2, which are selected by conducting extensive simulation studies based on some evolutionary algorithms [34–36] as shown in Fig. 6. The initial condition of the state vectors of (9) are set as the values adopted in a certain hydropower station as [0.1, 0.1, 0.1, 0.1, 0.1].

Table 1: The constants and uncertainties in HTGSBF model

System Constants			
$T_y = 0.1$ s	$T_a = 10.01$ s	$D = 2.00$	$h_{wi} = 0.05$
$E'_q = 1.35$	$V_s = 1.00$	$\tau_d = 1.15$	$\tau_q = 1.474$
$w_0 = 1.00$	$D = 2.00$	$T_{wp} = 9.35$ s	$T_{wi} = 1.82$ s
$e_{qxm} = -0.2901$	$e_{qym} = 0.8184$	$e_{qhm} = 0.7257$	$e_{hm} = -1.7179$
$e_{xm} = -1.0673$	$e_{ym} = 0.7713$		
System Uncertainties			
$d_1 = 0.003 \sin(t)$	$d_2 = 0.004 \sin(t)$		$d_3 = 0.005 \sin(t)$
$d_4 = 0.004 \cos(t)$	$d_5 = 0.003 \cos(t)$		

4.1 Fixed Point Stabilization

In this part, we choose the fixed reference output $x_d(t) = 1.0$. As shown in Fig. 7, all sliding mode controllers are able to reach the desired state x_d with only slight fluctuation because of the discontinuous item (15) under the time-variant disturbance d_m. Comparing to the results of CSMC approach, TTSMC and NTSMC methods have a faster response and smaller chattering magnitudes, which also can be seen from the sliding plot in Fig. 8. More details are provided in Tab. 3.

From the table and plots, we can see that the TTSMC controller has a shorter settling time while the NTSMC controller has a smaller percentage overshoot. Both TTSMC and NTSMC controllers have a better transient system response performance than the linear surface based CSMC controller.

Table 2: The parameters in controllers and saturation compensator

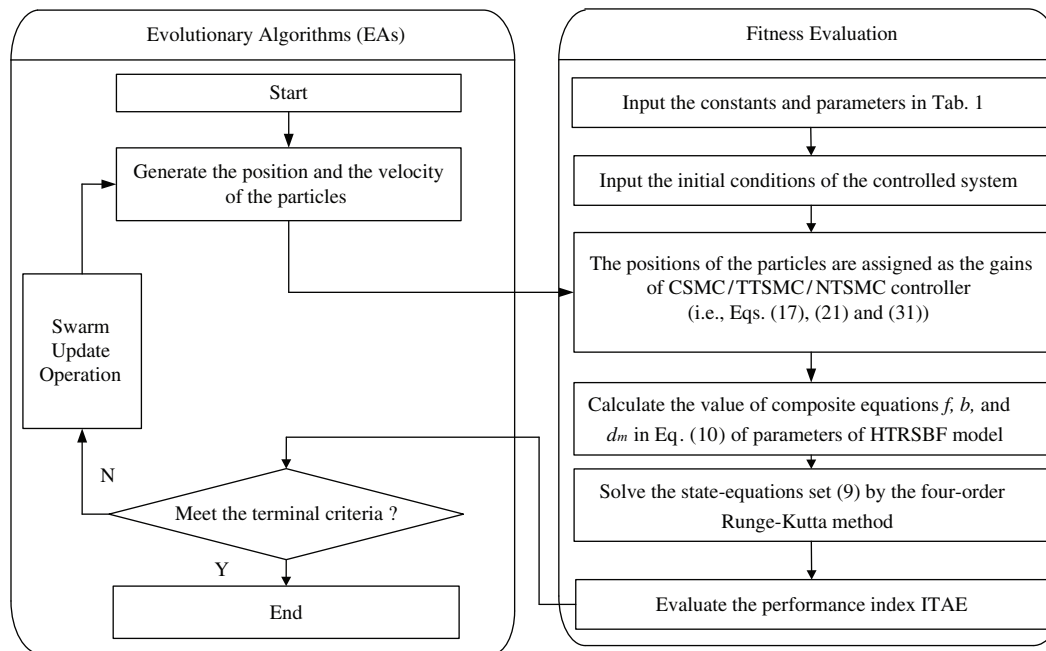| Saturation Compensator			
$c_1 = 50$	$c_2 = 50$	$u_{max} = 20$	$u_{min} = -20$
CSMC controller			
$c = 1$	$k_1 = 20$	(To have a fair comparison, $c = \alpha = \beta$)	
TTSMC controller			
$p_1 = 5$	$q_1 = 3$	$\beta = 1$	$k_2 = 20$
NTSMC controller			
$p_2 = 5$	$q_2 = 3$	$\alpha = 1$	$k_3 = 20$

Figure 6: The optimization process of CMSC/TTSMC/FTSMC controllers assisted with EAs

The sliding mode controller output u and saturation compensator output Δu are presented in Fig. 9. It can be seen that at the initial stage, the value of saturation compensator output Δu is very large, this is mainly due to the reason that the tracking error e of the reference output x_d and the actual output x_5 is the biggest at this moment. With the function of the controller and the saturation compensator, e gradually decreases, and then the output of the controller and the compensator decreases accordingly.

In practice, the parameters of hydraulic turbine are always varied due to the working conditions of HTGS system are usually changed from one status to another status [7], which is often caused by the external load variation. To examine the robustness property of TTSMC and NTSMC controllers, we study the effect of parameter variation on the dynamic response of the proposed control scheme under fixed point stabilization in this part. Without loss of generality, assume that all six basis transfer constants of the turbine, i.e., e_{hm}, e_{ym}, e_{xm}, e_{qhm}, e_{qym}, e_{qxm}, increase 50% over the original values at $7\ s \leq t \leq 10\ s$.
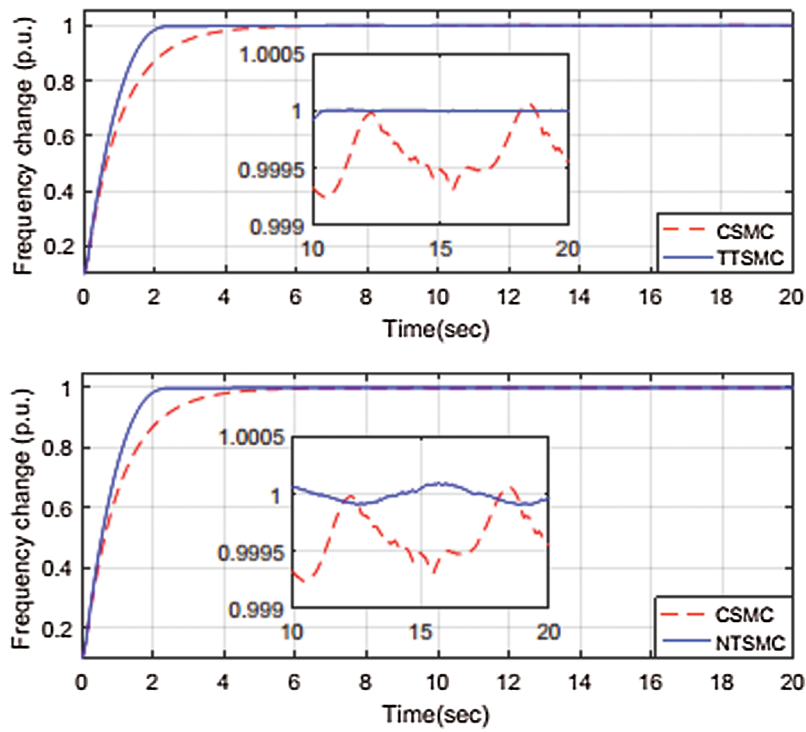
Figure 7: Frequency change of three sliding mode controllers under fixed point stabilization
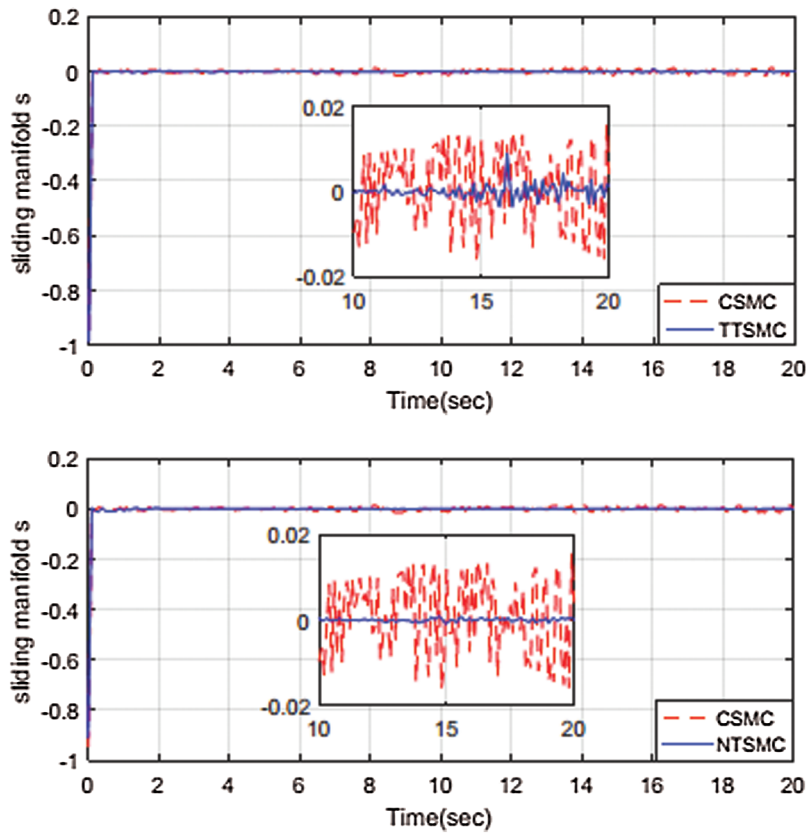

Figure 8: The manifold phase of three sliding mode controllers under fixed point stabilization

Table 3: The comparison of CSMC, TTSMC and NTSMC controllers under fixed point stabilization

	Rise time	Settling time	Overshoot	Steady-state error
CSMC	2.2164 s	4.0167 s	0.0110	0.00007554
TTSMC	1.3490 s	1.9850 s	0.0059	0.00000031
NTSMC	1.3515 s	1.9560 s	0.0018	0.00000179

The simulation results are shown in Fig. 10. As can be seen from Fig. 10, the TTSMC and NTSMC controllers have lower jumping amplitudes and shorter adjusting time, which means that the robustness of terminal sliding mode controllers are better than that of the conventional sliding mode controller. In other words, it demonstrates the effectiveness of the robust of our proposed sliding mode schemes during the parameter variations under fixed point stabilization.

4.2 Periodic Orbit Tracking

In this part, we take the reference output as $x_d(t) = 0.5 \sin(t)$. The CSMC, NTSMC and TTSMC controllers are employed to adjust the orbit of x_5 for comparison purpose. The frequency change and the tracking error, as well the controller effort and the compensator effort are presented in Figs. 11 and 12.

Fig. 13 and Tab. 4 list the corresponding performance indicators in total simulation time T, in which the following six indicators are considered to evaluate to the performance,

$$IAE = \int_0^T |e_r(t)|dt, \quad ITAE = \int_0^T t|e_r(t)|dt, \quad ITTAE = \int_0^T t^2|e_r(t)|dt$$

$$ISE = \int_0^T e_r^2(t)dt, \quad ITSE = \int_0^T te_r^2(t)dt, \quad ITTSE = \int_0^T t^2 e_r^2(t)dt \tag{34}$$

where $e_r = x_5 - x_d$ represents the tracking error.

Comparing the error tracking performance under periodic orbit tracking in Fig. 13 and Tab. 4, numerical results show that the TTSMC and NTSMC controllers are able to force the generator frequency tracking its reference promptly with littler chattering effect, which indicates that the system performance with terminal sliding mode controllers is much better than CSMC controller. The superiority of the TTSMC and NTSMC controllers are also shown in the plots of sliding mode manifold in Fig. 14.

Fig. 15 shows the effect of three controllers when six basis transfer constants of the turbine, i.e., e_{hm}, e_{ym}, e_{xm}, e_{qhm}, e_{qym}, e_{qxm}, increase 50% over the original values at $7\,s \leq t \leq 10\,s$. It is seen that all the sliding mode controllers are capable of bringing the tracking error back to zero, but the proposed TTSMC and NTSMC controllers have better convergence speed and smaller overshoot than the CSMC controller.

From the above analysis, it is obvious that the proposed TTSMC and NTSMC controllers not only can ensure the trajectory of tracking error converge to the equilibrium in a finite time, but also achieve some superior properties such as better convergence speed, the excellent system uncertainties rejection and the improvement of control accuracy. Besides that, the TTSMC can significantly reduce the chattering effects and maintain a faster response, while the NTSMC has a smaller settling time and overshoot percentage. Both of them outperforms conventional sliding mode controller at all indicators of regulation quality.

Tab. 5 lists the running time of all simulation experiments. From Tab. 5, it is seen that the simulation running time of terminal sliding mode controllers is a bit longer than that of conventional sliding mode controller. This is mostly owe to the exponential calculation in terminal sliding mode controller. Nevertheless, it should be noted that the chattering effects of sliding mode controllers for the HTGSBF
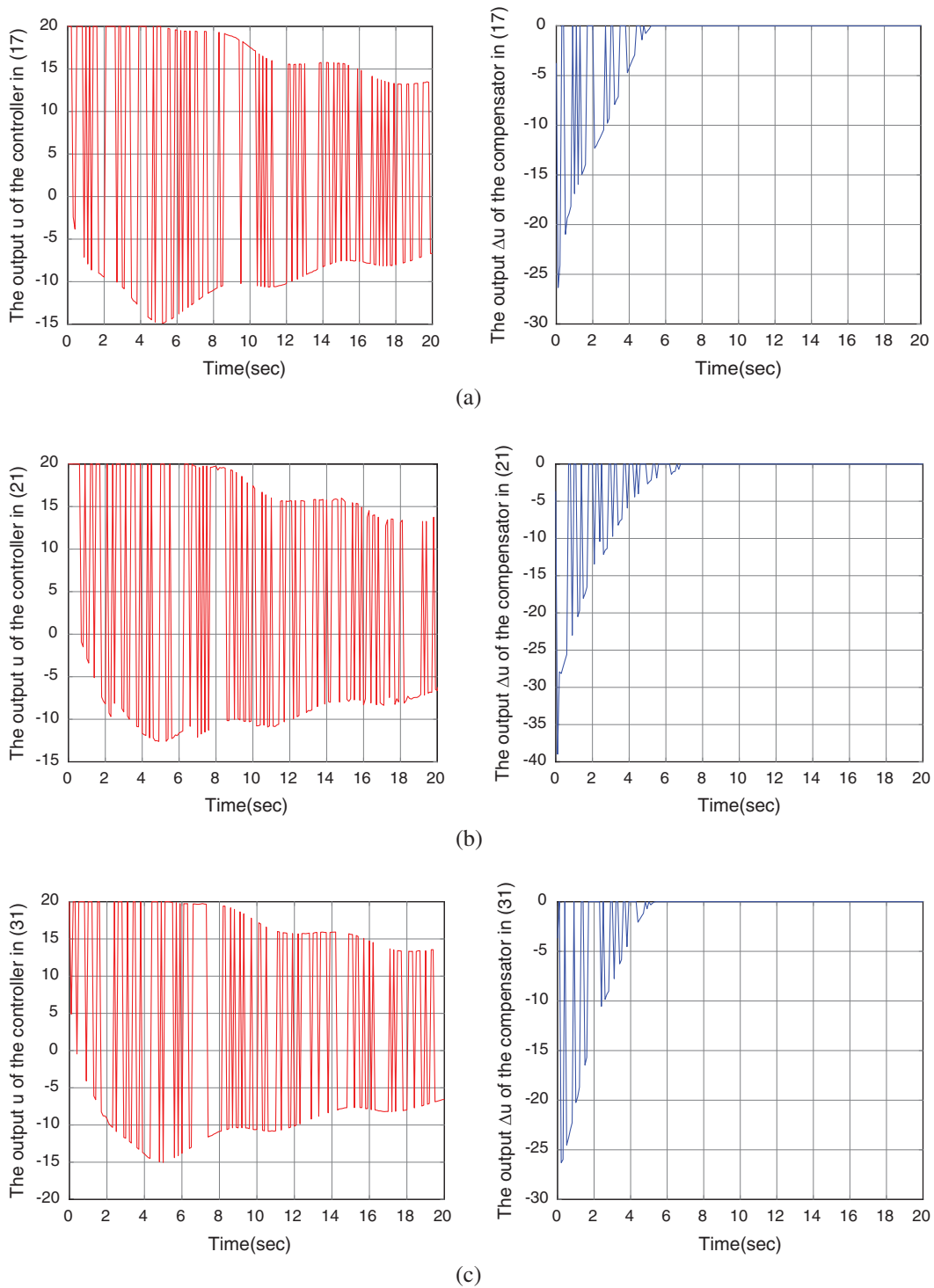
Figure 9: The outputs of u and Δu in three sliding mode controllers under fixed point stabilization. (a) The controller output and compensator effort of CSMC controller. (b) The controller output and compensator effort of TTSMC controller. (c) The controller output and compensator effort of NTSMC controller
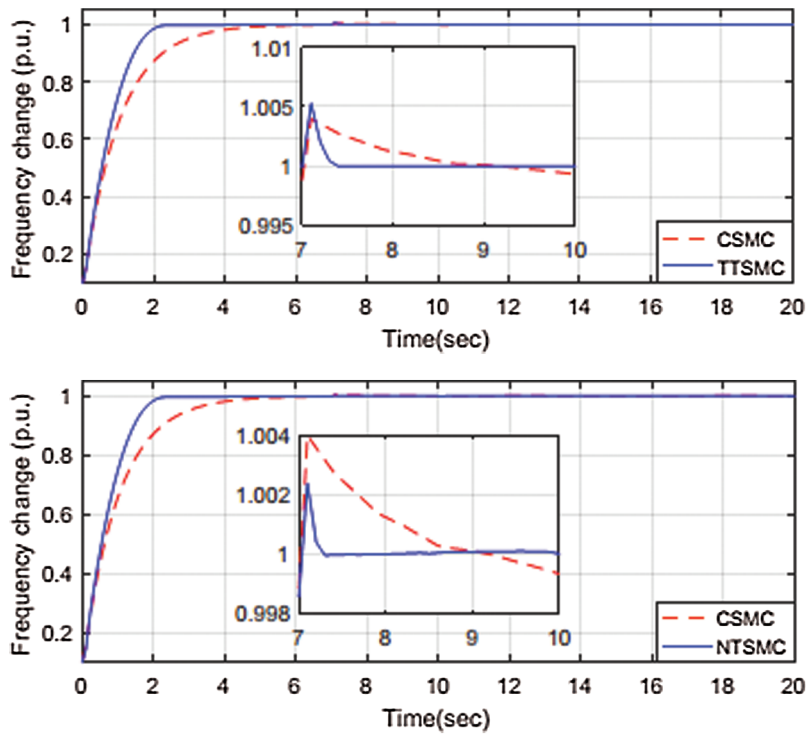
Figure 10: Dynamic performance under fixed point stabilization when six basis transfer constants of the turbine, i.e., e_{hm}, e_{ym}, e_{xm}, e_{qhm}, e_{qym}, e_{qxm}, increase 50% over the original values at $7s \leq t \leq 10s$
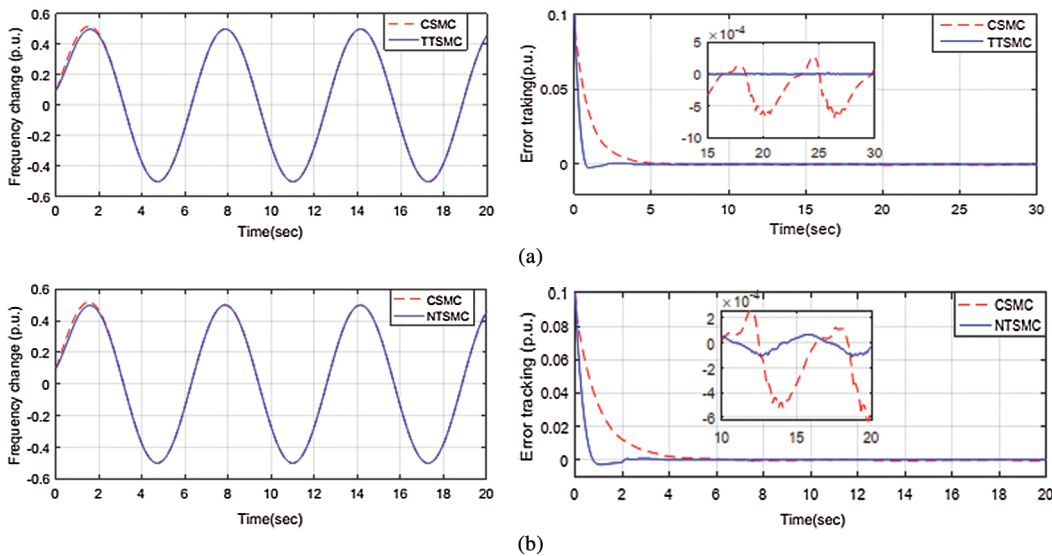

Figure 11: Frequency change and error tracking of three sliding mode controllers under periodic orbit tracking. (a) The results of frequency change and error tracking of CSMC and TTSMC controllers. (b) The results of frequency change and error tracking of CSMC and NTSMC controllers
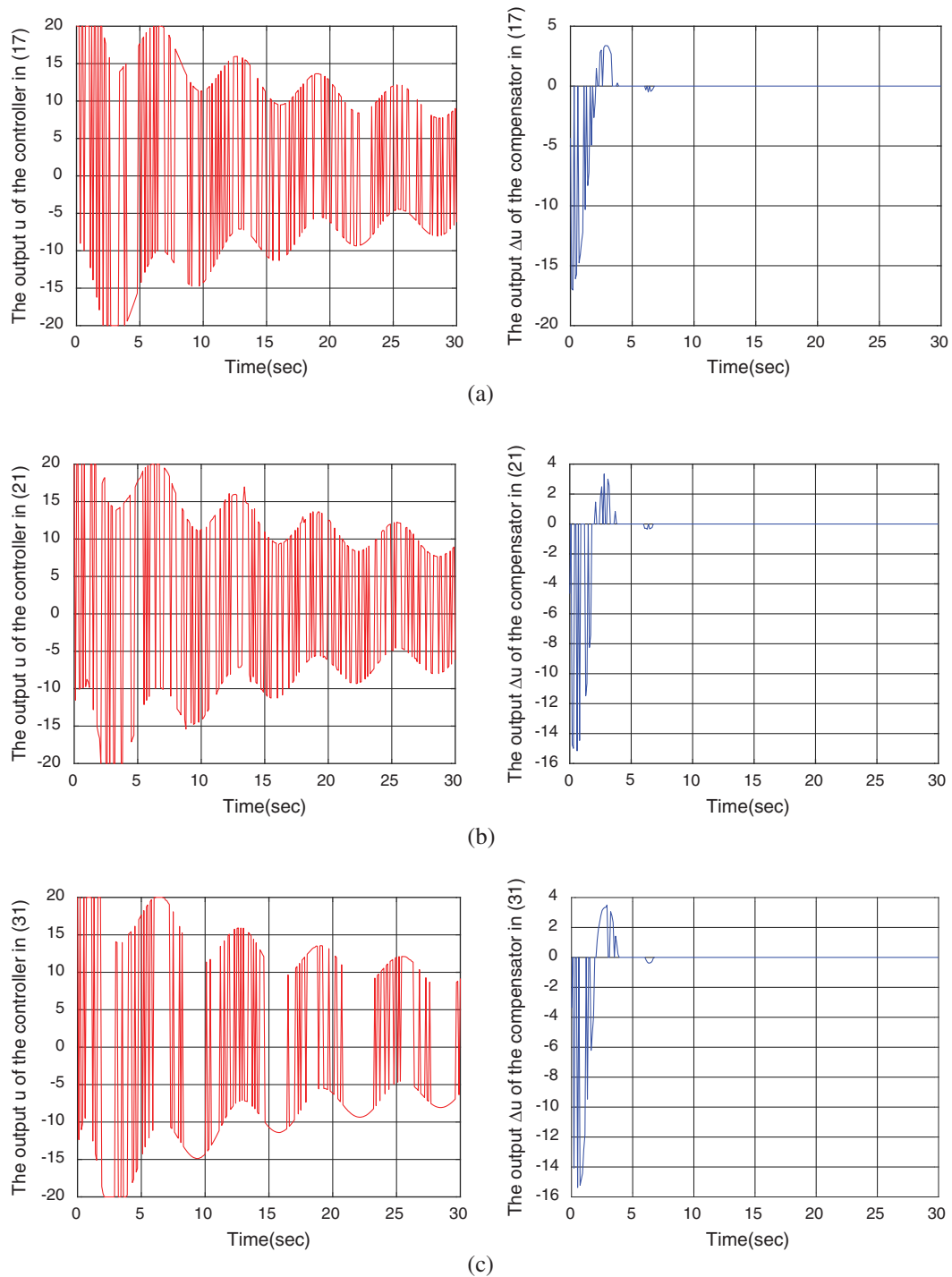
Figure 12: The outputs of u and Δu in sliding mode controllers under periodic orbit tracking. (a) The controller effort u and compensator effort Δu of CSMC controller. (b) The controller effort u and compensator effort Δu of TTSMC controller. (c) The controller output u and compensator effort Δu of NTSMC controller
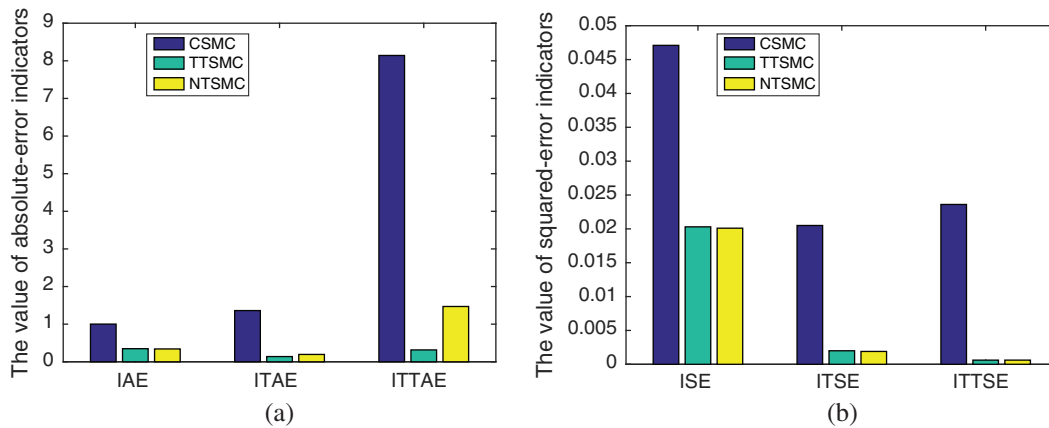
Figure 13: The performance comparison of three sliding mode controllers under periodic orbit tracking. (a) The absolute-error indicators of the controllers. (b) The squared-error indicators of the controllers

Table 4: The comparison of CSMC, TTSMC and NTSMC controllers under periodic orbit tracking

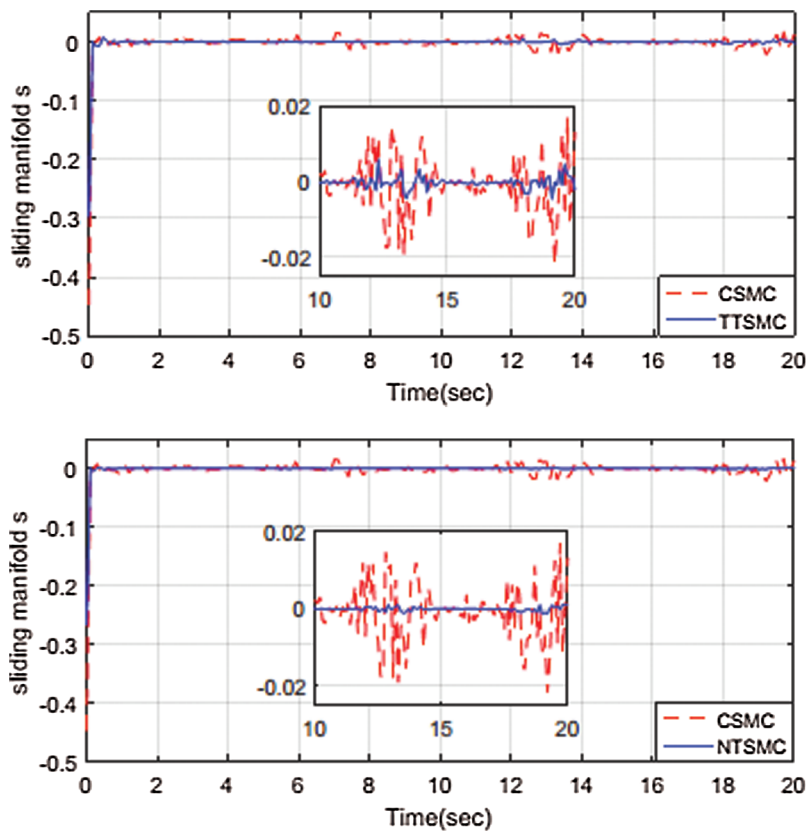|	IAE	ISE	ITAE	ITSE	ITTAE	ITTSE
CSMC	1.0016	0.0471	1.3611	0.0205	8.1422	0.023615
TTSMC	0.3477	0.0203	0.1386	0.0020	0.3152	0.000615
NTSMC	0.3409	0.0201	0.1953	0.0019	1.4697	0.000617

Figure 14: The manifold phase of three sliding mode controllers under periodic orbit tracking
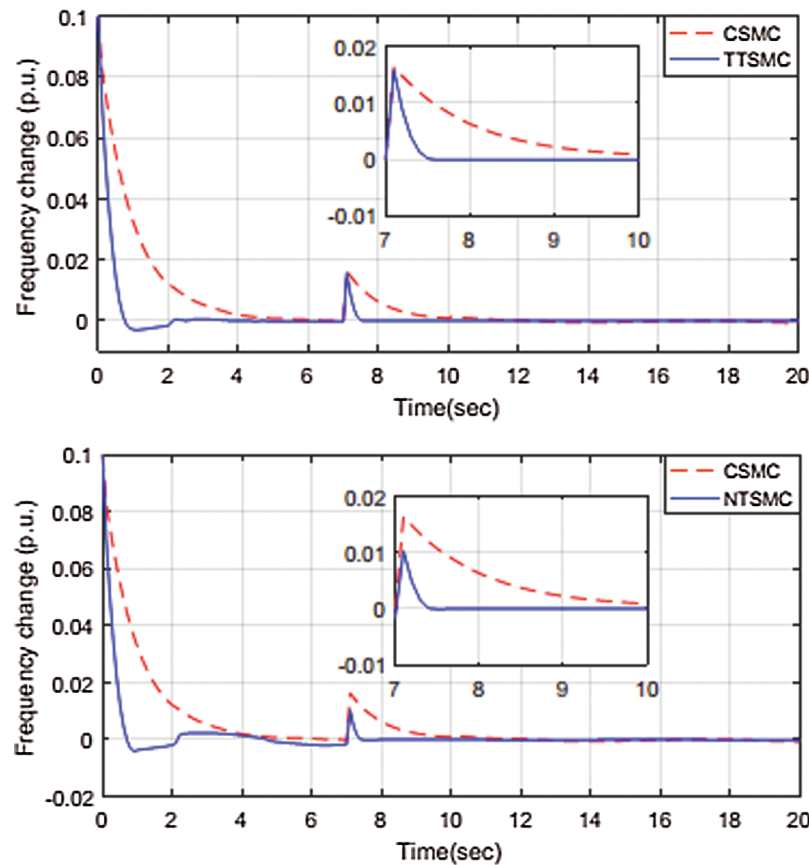
Figure 15: Dynamic performance under periodic orbit tracking when six basis transfer constants of the turbine, i.e., e_{hm}, e_{ym}, e_{xm}, e_{qhm}, e_{qym}, e_{qxm}, increase 50% over the original values at $7\ s \leq t \leq 10\ s$

Table 5: The running time of CSMC, TTSMC and NTSMC controllers in all simulation cases

	Case 1 (Fig. 4)	Case 2 (Fig. 7)	Case 3 (Fig. 9)	Case 4 (Fig. 11)
CSMC	5.1773 s	8.1561 s	66.3610 s	76.9897 s
TTSMC	16.8291 s	18.9028 s	97.1620 s	105.3390 s
NTSMC	10.1700 s	12.6678 s	81.6089 s	84.1569 s

Case 1: normal condition under fixed point stabilization; Case 2: robustness test under fixed point stabilization; Case 3: normal condition under periodic orbit tracking; Case 4: robustness test under periodic orbit tracking

cannot be eliminated completely, which is due to the reason that the discontinuous switching law in sliding mode controllers is the basis of the robustness of the dynamic response [37]. To make a balanced trade-off between reducing the chattering effect and enhancing system response performance to some extent, many excellent methods have been reported, see [38–41], and the references therein, which promotes the development and the improvement of sliding mode technology in industrial systems.

5 Discussions

Owing to the complex and special configurations in a hydro plant, the HTGS exhibits significant coupling properties with the interactions among mechanical, hydraulic, and electrical devices, which

enhance the difficulties in modeling and controlling this system. Up to now, it is still a challenging problem to establish the proper models and find the suitable control laws for the HTGS.

In this study, we first establish a new mathematical model of the HTGS, named HTGSBF model. In this model, bifurcated penstock and controller saturation is taken into account, which is very close to the prototype in Mangahao hydro plant [42]. Additionally, a two-order generator sub-model is adopted in the proposed model, where the relationships of electromagnetic torque and generator torque angle is considered. Besides that, in order to compensate the modelling errors caused by the actual model and prototype, the bounded system uncertainties d_1-d_5 are introduced in the nonlinear model. To the best of the authors' knowledge, few researchers have built the models of HTGS with considering so much factors in hydropower plants.

For the aspect of controlling HTGSBF model, this study introduces a novel control design of the HTGSBF model with respect to nonlinear sliding mode surface. Comparing the TTSMC and NTSMC controllers with the linear sliding mode surfaces listed in [7] and [13] (Actually, the CSMC controller is the variant of SMC controller in [7] and [13]), it is seen that there are two notable merits of terminal sliding mode controllers.

i) the HTGSBF model assisted with terminal sliding mode controllers can reach the equilibrium in a finite time, which can be found from theoretical analysis and simulation results;

ii) it speeds up the rate of convergence near an equilibrium. From (20), we can see that when the sliding mode manifold $s = 0$ is reached, $e = 0$ becomes a terminal attractor, i.e., $\dot{e} = -\beta e^{q_1/p_1}$, then it has:

$$t_s = -\frac{1}{\beta} \int_{e(0)}^{0} \frac{de}{e^{q_1/p_1}} = \frac{|e(0)|^{(1-q_1/p_1)}}{\beta(1 - q_1/p_1)}, \quad q_1 \neq p_1 \tag{35}$$

which implies that the term e^{q_1/p_1} makes the model converge to origin point with an exponential speed. On the other hand, $\dot{e} = -\beta e^{q_1/p_1}$ reduces to $\dot{e} = -\beta e$ for $q_1 = p_1$, which is same as the form of CSMC controller. In other words, CSMC is a special case of terminal sliding mode controllers.

Comparing to the input limitation approximation method listed in References [43,44], our approach is easy to be implemented. For the sake of completeness, the most often used PID controller and its variant controller (NPID) [45] have been introduced into the HTGSBF model in (9). The regulation law of PID controller is introduced as:

$$u_{PID} = k_p * e + k_i * \int_0^t e \, dt + k_d * \dot{e} \tag{36}$$

where k_p, k_i and k_d are the proportional gain, integral gain and derivative gain. The regulation law of NPID controller is defined as:

$$u_{NPID} = k_p * e + k_i * \int_0^t e \, dt + k_d * \dot{e} \quad where : \begin{cases} k_p = a_p + b_p(1 - sech(c_p \cdot e)) \\ k_i = a_i sech(b_i \cdot e) \\ k_d = a_d + b_d/(1 + c_d \exp(d_d \cdot e)) \end{cases} \tag{37}$$

where a_p, b_p, c_p, a_i, b_i, a_d, b_d, c_d and d_d are the parameters of NPID controller.

All the parameters in PID controller and NPID controller for HTGSBF model (9) are tuned by EAs [46–47] that similar to Fig. 7. Fig. 16 presents the comparison results. Tab. 6 lists the value of the corresponding indicators at $10\,s \leq t \leq 20\,s$ (The HTGSBF model is located at steady state during this period), which include maximum tracking errors (MTE), average tracking errors (ATE) and standard deviations of tracking errors (STE). The definition of these indicators are described as:
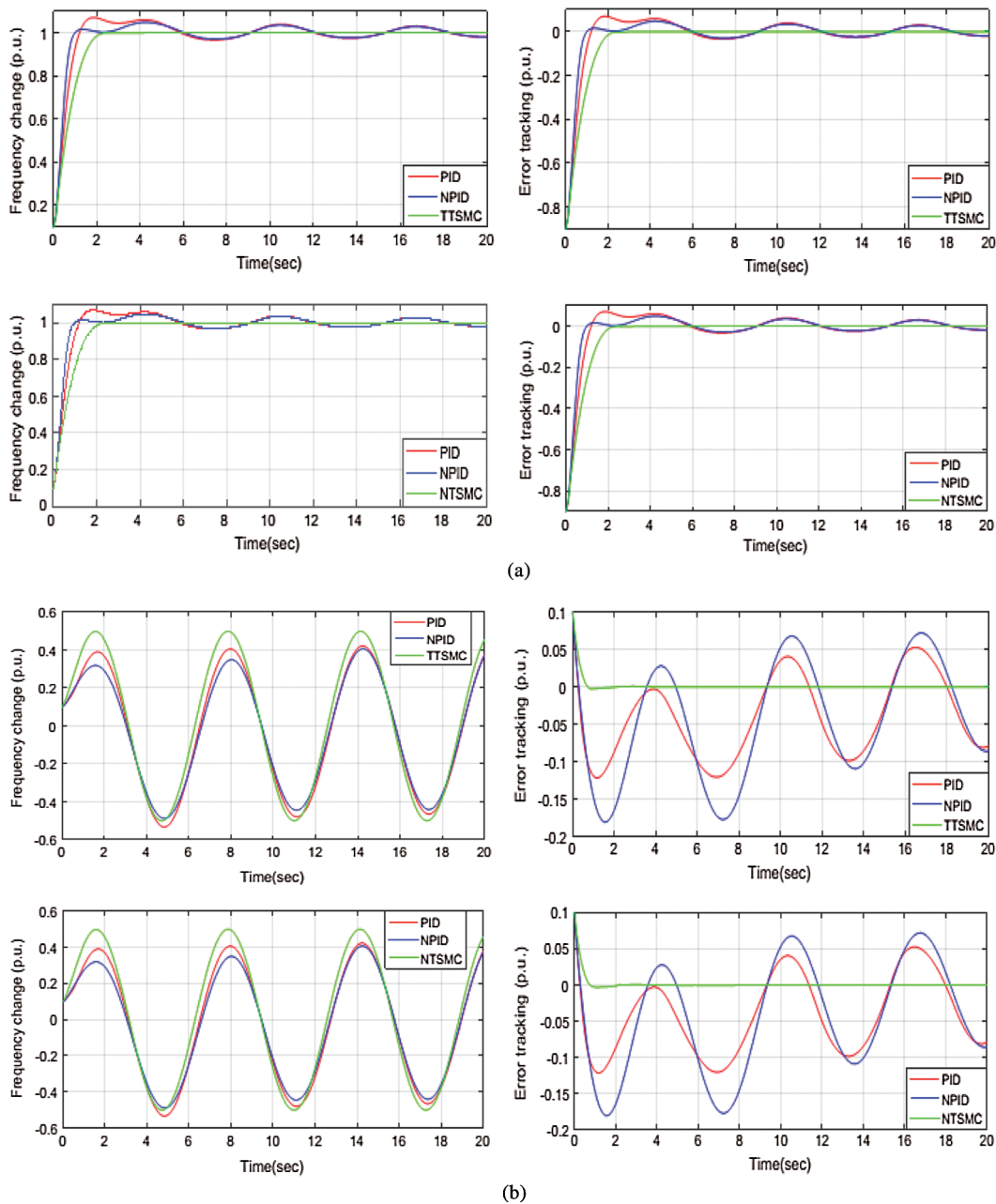
Figure 16: The comparison of PID controllers (including its variant) and terminal sliding mode controllers under fixed point stabilization and periodic orbit tracking. (a) The response and error trajectories of five controllers under fixed point stabilization. (b) The response and error trajectories of five controllers under periodic orbit tracking

Table 6: Quantitative analysis of different controllers under fixed point stabilization and periodic orbit tracking

The indicators of different type controllers under fixed point stabilization at $10\ s \le t \le 20\ s$				
	PID	NPID	TTSMC	NTSMC
MTE	0.0393	0.0345	0.0000986	0.0001012
ATE	0.0191	0.0179	0.0000056	0.0000498
STE	0.0101	0.0090	0.0000138	0.0000292
The indicators of different type controllers under periodic orbit tracking at $10\ s \le t \le 20\ s$				
	PID	NPID	TTSMC	NTSMC
MTE	0.0982	0.1088	0.0001123	0.00001480
ATE	0.0494	0.0564	0.0000473	0.00000143
STE	0.0278	0.0287	0.0000311	0.00000280

$$MTE = \max_{i \in \{1, 2, \cdots, m\}} |e(i)|, \quad ATE = \frac{1}{m} \sum_{i=1}^{m} |e(i)|, \quad STE = \sqrt{\frac{1}{m} \sum_{i=1}^{m} (|e(i)| - ATE)^2} \tag{38}$$

where $e(i) = x_5(i) - x_d(i)$ represents the adopted $i - th$ value of tracking error between the actual output x_5 and reference output x_d at $10\ s \le t \le 20\ s$.

From Fig. 16 and Tab. 6, we can see that the system performance of TTSMC and NTSMC controllers is much better than that of PID and NPID controller significantly, which proves the effectiveness and superiority of sliding mode control techniques over the commonly used PID in governing the hydro system.

From the above analysis, we can see that the terminal sliding mode control schemes outperform other comparison methods (such as CSMC controller, PID controller and NPID controller) in terms of all indicators, which demonstrates the effectiveness of our proposed control approaches. Although physical experiments are not introduced into this study because of the large size of hydropower plants and the constraints of experimental conditions, the numerical experiment result of this paper acts as a theoretical reference for the further study of hydropower plant control. In our future work, we will attempt to test the correctness of our numerical experiments by conducting scientific experiments and investigating the dynamic responses of HTGSBF model with full-load rated operating states or large fluctuation changes. Furthermore, to control the HTGSBF model more precisely, it is necessary to conducting a more refined simulation research and physical experiments on the coupling mechanism of hydraulic-mechanical-electrical system, especially for a specific study on the influence from turbine characteristics, in which stability of the operations is relatively more problematic [48–50]. In the next stage, we will perform a real application of the designed controller as shown in (17) and (21), and compare the results with commonly used PID controller. The critical point of the designed controller in practice is inherently an issue on the implementation of the terminal sliding mode control schemes for nonlinear system. Some researchers have published prominent and remarkable papers on this issue. So it is our future plan to realize the experimental terminal sliding mode controller in HTGS system. Furthermore, simulation results in this study still can be further improved by incorporating a high-order sliding surface into TTSMC and NTSMC, which has been attempted and proved to be effective by some pioneering engineers [51].

6 Conclusions

Although hydropower has the best payback ratio and highest efficiency in all electricity generating method due to the constant upgrading of turbine, penstock and reservoir design, most of the plant's control system are still using the classical PID technique developed in the 1960s. It limits the operating range of the controlled system such as specific water flow rate and reservoir level. As energy demands are increasing every day, it is necessary to develop a more flexible control system for the hydro plants to operate at different situations. The goal of this study is to design a novel nonlinear controller for the hydro plant in order to improve its ability to handle different operating conditions.

In this paper, a detailed nonlinear mathematical model that considers the effects of the bifurcated penstocks and um-modeled uncertainties is developed by using a five-order differential equations set, and the terminal sliding mode controller schemes are studied for governing the generator frequency change of this nonlinear HTGSBF model. In light of theoretical analysis and simulation results, four main significant conclusions can be obtained. Firstly, due to the exponential sliding mode surface, terminal sliding mode controller can provide a faster response and higher control accuracy than the conventional sliding mode controller for the HTGSBF model. Secondly, the chattering effect caused by the discontinuous sub-law control is dramatically reduced by using the terminal sliding mode technique. Thirdly, terminal sliding mode controller owns a superior robustness property in against parameter variation. Fourthly, comparing to the current most used PID controller and its variants, terminal sliding mode controllers perform much better in terms of maximum tracking errors, average tracking errors, and standard deviations of tracking errors.

Conflicts of Interest: The authors declare that they have no conflicts of interest to report regarding the present study.

References

1. Strah, B., Kuljaca, O., Vukic, Z. (2005). Speed and active power control of hydro turbine unit. *IEEE Transactions on Energy Conversion, 20(2),* 424–434. DOI 10.1109/TEC.2004.837278.

2. Wang, W., Beddard, A., Barnes, M., Marjanovic, O. (2014). Analysis of active power control for VSC-HVDC. *IEEE Transactions on Power Delivery, 29(4),* 1978–1988. DOI 10.1109/TPWRD.2014.2322498.

3. Chen, D., Ding, C., Ma, X., Yuan, P., Ba, D. (2013). Nonlinear dynamical analysis of hydro-turbine governing system with a surge tank. *Applied Mathematical Modelling, 37(14),* 7611–7623. DOI 10.1016/j.apm.2013.01.047.

4. Xu, B., Wang, F., Chen, D., Zhang, H. (2016). Hamiltonian modeling of multi-hydro-turbine governing systems with sharing common penstock and dynamic analyses under shock load. *Energy Conversion and Management, 108,* 478–487. DOI 10.1016/j.enconman.2015.11.032.

5. Chen, Z., Yuan, X., Ji, B., Wang, P., Tian, H. (2014). Design of a fractional order PID controller for hydraulic turbine regulating system using chaotic non-dominated sorting genetic algorithm II. *Energy Conversion and Management, 84,* 390–404. DOI 10.1016/j.enconman.2014.04.052.

6. Chen, Z., Yuan, Y., Yuan, X., Huang, Y., Li, X. et al. (2015). Application of multi-objective controller to optimal tuning of PID gains for a hydraulic turbine regulating system using adaptive grid particle swam optimization. *ISA Transactions, 56,* 173–187. DOI 10.1016/j.isatra.2014.11.003.

7. Yuan, X., Chen, Z., Yuan, Y., Huang, Y., Li, X. et al. (2016). Sliding mode controller of hydraulic generator regulating system based on the input/output feedback linearization method. *Mathematics and Computers in Simulation, 119,* 18–34. DOI 10.1016/j.matcom.2015.08.020.

8. Guo, W., Yang, J., Chen, J., Wang, M. (2016). Nonlinear modeling and dynamic control of hydro-turbine governing system with upstream surge tank and sloping ceiling tailrace tunnel. *Nonlinear Dynamics, 84(3),* 1383–1397. DOI 10.1007/s11071-015-2577-0.

9. Li, H., Chen, D., Zhang, H., Wang, F., Ba, D. (2016). Nonlinear modeling and dynamic analysis of a hydro-turbine governing system in the process of sudden load increase transient. *Mechanical System and Signal Processing, 80,* 414–428. DOI 10.1016/j.ymssp.2016.04.006.

10. Wang, F., Chen, D., Xu, B., Zhang, H. (2016). Nonlinear dynamics of a novel fractional-order Francis hydro-turbine governing system with time delay. *Chaos, Solitons & Fractals, 91,* 329–338. DOI 10.1016/j.chaos.2016.06.018.

11. Zhang, H., Chen, D., Wu, C., Wang, X. (2018). Dynamics analysis of the fast-slow hydro-turbine governing system with different time-scale coupling. *Communications in Nonlinear Science and Numerical Simulation, 54,* 136–147. DOI 10.1016/j.cnsns.2017.05.020.

12. Liang, J., Yuan, X., Yuan, Y., Chen, Z., Li, Y. (2017). Nonlinear dynamic analysis and robust controller design for Francis hydraulic turbine regulating system with a straight-tube surge tank. *Mechanical System and Signal Processing, 85,* 927–946. DOI 10.1016/j.ymssp.2016.09.026.

13. Xu, B., Chen, D., Venkateshkumar, M., Xiao, Y., Yue, Y. et al. (2019). Modeling a pumped storage hydropower integrated to a hybrid power system with solar-wind power and its stability analysis. *Applied Energy, 248,* 446–462. DOI 10.1016/j.apenergy.2019.04.125.

14. Yuan, X., Chen, Z., Yuan, Y., Huang, Y. (2015). Design of fuzzy sliding mode controller for hydraulic turbine regulating system via input state feedback linearization method. *Energy, 93,* 173–187. DOI 10.1016/j.energy.2015.09.025.

15. Laghari, J. A., Mokhlis, H., Bakar, A. H. A. (2014). A fuzzy based load frequency control for distribution network connected with mini hydro power plant. *Journal of Intelligent and Fuzzy Systems, 26(3),* 1301–1310. DOI 10.3233/IFS-130816.

16. Yi, Y., Zhang, Z., Chen, D., Zhou, R., Patelli, E. et al. (2018). State feedback predictive control for nonlinear hydro-turbine governing system. *Journal of Vibration and Control, 24(21),* 4945–4959.

17. Zhang, R., Chen, D., Yao, W. (2017). Non-linear fuzzy predictive control of hydroelectric system. *IET Generation, Transmission & Distribution, 11(8),* 1966–1975. DOI 10.1049/iet-gtd.2016.1300.

18. Venayagamoorthy, G. K., Harley, R. G. (2001). A continually online trained neurocontroller for excitation and turbine control of a turbogenerator. *IEEE Transactions on Energy Conversion, 16(3),* 261–269. DOI 10.1109/60.937206.

19. Ding, X., Sinha, A. (2011). Sliding mode/H∞ control of a hydro-power plant. *American Control Conference, IEEE,* 520–5206.

20. Komurcugil, H. (2012). Adaptive terminal sliding-mode control strategy for DC-DC buck converters. *ISA Transactions, 51(6),* 673–681. DOI 10.1016/j.isatra.2012.07.005.

21. Wu, Y., Zuo, J., Sun, L. (2017). Adaptive terminal sliding mode control for hypersonic flight vehicles with strictly lower convex function based nonlinear disturbance observer. *ISA Transactions, 71,* 215–226. DOI 10.1016/j.isatra.2017.08.008.

22. Safa, A., Abdolmalaki, R. Y., Shafiee, S., Sadeghi, B. (2018). Adaptive nonsingular terminal sliding mode controller for micro/nanopositioning systems driven by linear piezoelectric ceramic motors. *ISA Transactions, 77,* 122–132. DOI 10.1016/j.isatra.2018.03.027.

23. Ma, Z., Yu, X. (1997). Terminal sliding mode control of MIMO linear systems. *IEEE Transactions on Circuits Systems-I, 44(11),* 1065–1070. DOI 10.1109/81.641769.

24. Feng, Y., Yu, X., Man, Z. (2002). Non-singular terminal sliding mode control of rigid manipulators. *Automatica, 38(12),* 2159–2167. DOI 10.1016/S0005-1098(02)00147-4.

25. Chen, Z., Yuan, X., Tian, H., Ji, B. (2014). Improved gravitational search algorithm for parameter identification of water turbine regulation system. *Energy Conversion and Management, 78,* 306–315. DOI 10.1016/j.enconman.2013.10.060.

26. Xu, C., Qian, D. (2015). Governor design for a hydropower plant with an upstream surge tank by GA-based fuzzy reduced-order sliding mode. *Energies, 8(12),* 13442–13457. DOI 10.3390/en81212376.

27. Chen, Z., Yuan, X., Yuan, Y., Iu, H., Fernando, T. (2017). Parameter identification of integrated model of hydraulic turbine regulating system with uncertainties using three different approaches. *IEEE Transactions on Power Systems, 32(5),* 3482–3491. DOI 10.1109/TPWRS.2016.2639293.

28. USGS. 2015. (2015). Environment Canada: hydroelectric power water use—typical hydro-electric power plant. *http://ga.water.usgs.gov/edu/wuhy.html*.

29. Perruquetti, W., Barbot, J. P. (2002). *Sliding mode control in engineering*. Boca Raton: CRC Press.

30. Li, S., Zhou, M., Yu, X. (2013). Design and implementation of terminal sliding mode control method for PMSM speed regulation system. *IEEE Transactions on Industry Information, 9(4),* 1879–1891. DOI 10.1109/TII.2012.2226896.

31. Bandyopadhyay, B., Sivaramakrishnan, J., Sarah, S. K. (2013). *Advances in sliding mode control: concept, theory and implementation*. Germany: Springer Press.

32. Corradini, M., Cristofaro, A. (2018). Nonsingular terminal sliding-mode control of nonlinear planar systems with global fixed-time stability guarantees. *Automatica, 95,* 561–565. DOI 10.1016/j.automatica.2018.06.032.

33. Lucero, T. L. A. (2010). *Hydro turbine and governor modeling (Master Thesis)*. Norwegian University of Science and Technology, Trondheim, Norwegian.

34. Yuan, X., Tan, Q., Lei, X., Yuan, Y., Wu, X. (2017). Wind power prediction using hybrid autoregressive fractionally integrated moving average and least square support vector machine. *Energy, 129,* 122–137. DOI 10.1016/j.energy.2017.04.094.

35. Yuan, X., Zhang, Y., Yuan, Y. (2008). Improved self-adaptive chaotic genetic algorithm for hydrogeneration scheduling. *Journal of Water Resources Planning and Management-ASCE, 134(4),* 319–325. DOI 10.1061/(ASCE)0733-9496(2008)134:4(319).

36. Yuan, X., Ji, B., Yuan, Y., Ikram, R., Zhang, X. et al. (2015). An efficient chaos embedded hybrid approach for hydro-thermal unit commitment problem. *Energy Conversion and Management, 91,* 225–237. DOI 10.1016/j.enconman.2014.12.021.

37. Liu, J., Wang, X. (2012). *Advanced sliding mode control for mechanical systems*. Germany: Springer Press.

38. Moharana, A., Dash, P. (2010). Input-output linearization and robust sliding mode controller for the VSC-HVDC transmission link. *IEEE Transactions on Power Delivery, 25(3),* 1952–1961. DOI 10.1109/TPWRD.2010.2042469.

39. Lin, J., Huang, S., Shih, K. R. (2003). Application of sliding surface enhanced fuzzy control for dynamic state estimation of a power system. *IEEE Transactions on Power Systems, 18(2),* 570–577. DOI 10.1109/TPWRS.2003.810894.

40. Tapia, A., Bernal, M., Fridman, L. (2017). Nonlinear sliding mode control design: an LMI approach. *System Control Letters, 104,* 38–44. DOI 10.1016/j.sysconle.2017.03.011.

41. Efimov, D., Polyakov, A., Fridman, L., Perruquetti, W., Richard, J. P. (2015). Delayed sliding mode control. *Automatica, 64,* 37–43. DOI 10.1016/j.automatica.2015.10.055.

42. Hannett, L. N., Feltes, J. W. (1999). Modeling and control tuning of a hydro station with units sharing a common penstock section. *IEEE Transactions on Power Systems, 14(4),* 1407–1414. DOI 10.1109/59.801904.

43. Chen, M., Ge, S., Ren, B. (2011). Adaptive tracking control of uncertain MIMO nonlinear systems with input constraints. *Automatica, 47(3),* 452–465. DOI 10.1016/j.automatica.2011.01.025.

44. Wang, H., Chen, B., Liu, X., Liu, K. (2013). Robust adaptive fuzzy tracking control for pure-feedback stochastic nonlinear systems with input constraints. *IEEE Transactions on Cybernetics, 43(6),* 2093–2104. DOI 10.1109/TCYB.2013.2240296.

45. Li, C., Zhang, N., Lai, X., Zhou, J., Xu, Y. (2017). Design of a fractional-order PID controller for a pumped storage unit using a gravitational search algorithm based on the Cauchy and Gaussian mutation. *Information Sciences, 396,* 162–181. DOI 10.1016/j.ins.2017.02.026.

46. Yuan, X., Zhang, B., Wang, P., Liang, J., Yuan, Y. et al. (2017). Multi-objective optimal power flow based on improved strength Pareto evolutionary algorithm. *Energy, 122,* 70–82. DOI 10.1016/j.energy.2017.01.071.

47. Yuan, X., Wang, Y., Xie, J., Qi, X., Nie, H. et al. (2010). Optimal self-scheduling of hydro producer in the electricity market. *Energy Conversion and Management, 51(12),* 2523–2530. DOI 10.1016/j.enconman.2010.05.017.

48. Yang, Y., Hua, C., Li, J., Guan, X. (2016). Fixed-time backstepping control design for high-order strict-feedback non-linear systems via terminal sliding mode. *IET Control Theory and Applications, 11(8),* 1184–1193.

49. Ning, D., Sun, S., Wei, L., Zhang, B., Du, H. et al. (2017). Vibration reduction of seat suspension using observer based terminal sliding mode control with acceleration data fusion. *Mechatronics, 44,* 71–83. DOI 10.1016/j.mechatronics.2017.04.012.

50. Yazici, I., Yaylaci, E. (2016). Fast and robust voltage control of DC-DC boost converter by using fast terminal sliding mode controller. *IET Power Electronics, 9(1),* 120–125. DOI 10.1049/iet-pel.2015.0008.

51. Lu, E., Li, W., Yang, X., Liu, Y. (2019). Anti-disturbance speed control of low-speed high-torque PMSM based on second-order non-singular terminal sliding mode load observer. *ISA Transactions, 88,* 142–152. DOI 10.1016/j.isatra.2018.11.028.